Available online at www.sciencedirect.com

ScienceDirect

Procedia CIRP 111 (2022) 340–344

www.elsevier.com/locate/procedia

12th CIRP Conference on Photonic Technologies [LANE 2022], 4-8 September 2022, Fürth, Germany

In-situ monitoring of the Laser Powder Bed Fusion build process via bi-chromatic optical tomography

T. Becker[a,*], S. J. Altenburg[a], N. Scheuschner[a], P. P. Breese[a], C. Metz[b], K. Hilgenberg[a]

C. Maierhofer[a]

[a]*Bundesanstalt für Materialforschung und -prüfung (BAM), Unter den Eichen 87, 12205 Berlin, Germany*
[b]*ThetaScan GmbH, Thyssenstraße 183a, 46535 Dinslaken, Germany*

* Corresponding author. Tel.: +49 30 8104 - 5596. *E-mail address:* tina.becker@bam.de

Abstract

As metal additive manufacturing (AM) is entering industrial serial production of safety relevant components, the need for reliable process qualification is growing continuously. Especially in strictly regulated industries, such as aviation, the use of AM is strongly dependent on ensuring consistent quality of components. Because of its numerous influencing factors, up to now, the metal AM process is not fully controllable. Today, expensive part qualification processes for each single component are common in industry.
This contribution focusses on bi-chromatic optical tomography as a new approach for AM in-situ quality control. In contrast to classical optical tomography, the emitted process radiation is monitored simultaneously with two temperature calibrated cameras at two separate wavelength bands. This approach allows one to estimate the local maximum temperatures during the manufacturing process, thus increases the comparability of monitoring data of different processes. A new process information level at low investment cost is reachable, compared to, e.g., infrared thermography.

Keywords: Additive Manufacturing; L-PBF; in-process monitoring; optical tomography

1. Introduction

Additive Manufacturing (AM) as a non-conventional manufacturing method enables the production of components with a high degree of design freedom directly from a CAD file. Hereby, the aimed component design is sliced digitally, and the part is built up layer by layer. The high demand for AM technologies is reflected in the growing AM market and still increasing investments in AM startups.[1]

With its beginnings in the mid-1980s, AM has already been investigated for a long time. Due to its complex physical processes, especially AM for metallic components is still not a fully mastered manufacturing method. In the field of metal AM, powder bed fusion systems e.g., laser powder bed fusion (L-PBF), are most utilized.[2] Here, components are manufactured layer-wise by a laser or electron beam from a powder bed. The powder is molten selectively and the component is formed of the solidified melt.

The wide acceptance and implementation of L-PBF is slowed by the lack of knowledge of the highly complex melting and solidification processes and the lack of available process monitoring. The high interest in the field of in-process monitoring for the L-PBF process is shown in the number of publications and research programs on this subject.[3,4]

One camera-based in-process monitoring approach is the optical tomography (OT). Here, spatially resolved long-time exposure layer-images of the manufacturing process are taken

10.1016/j.procir.2022.08.035

by an off-axis positioned camera operating in the near infrared spectrum (NIR). [5,6,7]

To gain high confidence in part quality and to compare different L-PBF processes, knowledge of the surface temperature is required. [4] Due to process intrinsic factors e.g., spattering, a vapor plume above the molten pool and changing emissivity values ε, the interpretation or temperature correlation of the process data recorded by a camera operating at a single wavelength window is challenging.

A possible route to overcome the influence of the changing emissivity ε is the monitoring of two separate wavelength ranges. Following this approach, Pavlov et al. [8] and Furumoto et al. [9] showed with two-color pyrometric measurements melt pool temperatures in the range of 900 - 2600°C for stainless steel [8] and 1520 - 1810°C for a steel-cupper-nickel alloy [9] for L-PBF set-ups. On-axis bi-chromatic monitoring approaches are presented by Sigma labs Inc. [10] and Hooper [11].

In this paper, the authors present an approach for the combination of the spatially resolved optical tomography with bi-chromatic surface temperature measurement. To this end, two industrial cameras for the visible light range equipped with bandpass filters transmitting at two different wavelength windows were integrated in a single optical path. An initial experiment at a commercial L-PBF printer had been performed and the used optical set-up was characterized by comparative measurements at calibrated light sources. Finally, conclusions were drawn for further development.

2. Approach

Even if optical tomography has no intrinsic time resolution, it can be assumed that most of the signal comes from the moment of highest temperature due to the ~T^4 dependence of the total emitted radiance, described by the Stefan-Boltzmann law. Considering the molten pool as a gray body with an emissivity in the range of $\varepsilon = 0.2$ [13], the specific spectral radiance $M_\lambda(\lambda,T)$ can be calculated according to the Planck's law as the product of the specific spectral radiance of an ideal black body $M_\lambda^0(\lambda,T)$ with the spectral emissivity ε of the molten pool.

The signal intensity I of one camera can be calculated as a function of the temperature by integrating the specific spectral radiance $M_\lambda(\lambda,T)$ of the monitored molten pool, the spectral transmittance $\tau(\lambda)$ of the optical set-up components, e.g., lenses and filters, the spectral sensitivity $S(\lambda)$ of the camera detector, and a device specific correction factor c, as shown in equation 1.

$$I(\lambda,T) = c \int\int \varepsilon(\lambda,T) \cdot M_\lambda^0\big(\lambda,T(t)\big) \cdot \tau(\lambda) \cdot S(\lambda) \cdot \, d\lambda \, dt \qquad (1)$$

The exact emissivity of the molten pool in the L-PBF process is unknown and prone to unpredictable influences such as the oxidation-level and the keyhole depression. A numerical determination of equation 1 is therefore not feasible for temperature estimation.

By using narrow bandpass filters at wavelengths $\lambda_{1/2}$ and assuming the main influence of only the maximum temperature T_{max}, the signal intensities of the two cameras can be calculated by equation 2.

$$I_{1/2} = k \cdot \varepsilon_{1/2} \cdot M_\lambda^0\big(\lambda_{1/2}, T_{max}\big) \cdot \, \tau\big(\lambda_{1/2}\big) \cdot S\big(\lambda_{1/2}\big) \qquad (2)$$

Now, by calculating the quotient of the two signal intensities I_1 and I_2, the weaker assumption of a constant ratio of the two occurring emissivities can be used to calculate the maximum temperature implicitly by means of a look-up-table. Therefore, the bi-chromatic approach was used in this paper.

3. Experimental set-up

3.1. Optical sensor system and test set-up

To monitor the L-PBF process spatially resolved at two sharply separated wavelength ranges, a set-up consisting of two identical monochromatic CMOS cameras with a resolution of 24.4 mega pixel and a pixel size of 2.74 µm x 2.74 µm, equipped with two different bandpass filters, as shown in figure 1b, were used.

The two cameras were mounted via a beam splitter to a lens to focus on the lop-layer of the AM build process. In addition, both focal lengths of the cameras were adjusted independently to account for the different optical paths in the two used wavelengths ranges. Bandpass filters with central wavelengths of 500 nm and 550 nm and a full width at half maximum (FWHM) of 25 nm were chosen for test purposes. This set-up enabled recordings of both cameras without over- or underexposure.

An additional median blurring was applied to one recorded and matched image set, to align the resolutions. To further adjust the incident light for both cameras and to block the manufacturing laser, a shortpass filter with cut-off wavelength 750 nm, an aperture and a temperature-balancing filter were used. The transmittance curves of the used filters are shown in figure 1b.

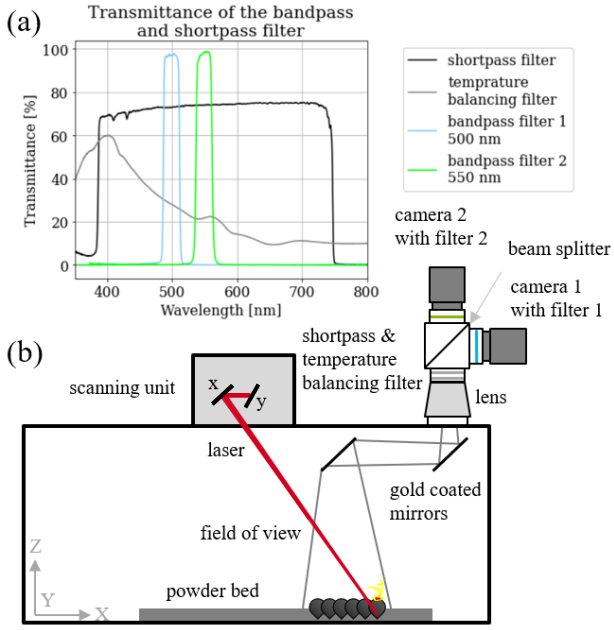

Fig. 1. (a)Transmittance curves of the used filters and (b) schematic of the test set-up with the optical sensor system.

To test the sensor set-up at real process conditions, it was mounted on top of a commercial metal 3D printer (SLM280HL, SLM Solutions AG) above a sapphire window in the chambers ceiling. To allow for a nearly perpendicular view of the off axis positioned camera system two gold coated mirrors were used to guide the field of view to a section of the powder bed, as illustrated in figure 1.

For the evaluation of the sensor set-up, the scanning process of a cubic 8 mm x 8 mm x 25 mm sample, as shown in figure 2a, was monitored. The component was built out of the nickel-based alloy Haynes282 and scanned with a laser power of P_L = 225 W, scan speed v = 1100 mm/s and a layer thickness d_s = 40 µm. In the component, defined areas with varied laser power of P_L = ±10 %, ±20 %, ±40 % of the standardly used parameter were inserted to test the capability of the sensor set-up to detect different volume energies E_V.

3.2. Calibration set-up

To calculate temperature values from the measured signals, a detailed knowledge about the optical properties of the used sensor set-up is mandatory. The components of the sensor set-up were therefore optically characterized.

The spectral transmittance τ(λ) of the used bandpass filters, shortpass filter, temperature balancing filter and lens system were measured by use of a spectrometer (USB2000+UV-VIS-ES, Ocean Insight inc.) in combination with a calibrated halogen lamp and an integrating sphere (K-ISS-30_VA_V01, Gigahertz-Optik) with known spectral specific radiance $M_\lambda(\lambda)$ and a correlated color temperature of T = 3190 K in the visible range between 360 nm – 750 nm.

To characterize the spectral sensitivity S(λ) of the camera sensors, the cameras were positioned in front of the calibrated light source with different narrow bandpass filters in the range between 400 nm to 725 nm with an FWHM of 25 nm each and the actual spectral sensitivities S(λ) of the camera sensors were determined. The determined spectral sensitivity S(λ) was assigned to the corresponding central wavelengths of the respective filters.

A calibrated black body radiator (BB) for temperatures up to 1200°C (PYROTHERM CS 1200, DIAS Infrared GmbH) was used to validate the theoretically determined temperature look-up-table of the sensor set-up used. Since the BB was not calibrated for the VIS range, a correction-curve determined by comparative measurements with the calibrated halogen lamp for the VIS range had been used.

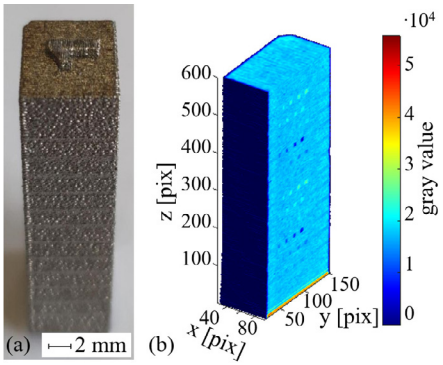

Fig. 2. Monitored component (a) L-PBF manufactured component and (b) monitoring data in gray values of one camera.

4. Results and Discussion

In figure 3, the calibration curves for the interpretation of the measured signal intensities ratio I_1/I_2 of the sensor set-up for different bandpass filter combinations is shown. The plotted lines represent the theoretically calculated signal ratios in relation to the monitored object maximum temperature. The experimentally measured signal intensity ratios I_1/I_2 for the temperatures T = 1273 K, 1473 K, measured at the black body radiator and T = 3190 K, measured at the halogen lamp are marked with crosses of the respective color.

Though there are outliers with higher deviations for the 650 nm/550 nm calibration measurements, the mean deviation of the experimental measured and calculated values is e_{mean} = 2%. For a measured temperature of T = 2900 K that means a measurement uncertainty of ±65 K.

This shows the capability of the sensor set-up to measure temperature as expected by the molten pool in the L-PBF process by means of measuring emitted light in the VIS range.

The expected accuracy and measurement uncertainty strongly depends on the temperature range and filter combination. The sensor set-up can be adapted for different measurement tasks, by choosing the best fitting bandpass filter combination. Since a combination of 500 nm/550 nm was used in the initial experiment, the 500 nm/550 nm curve was used as look-up-table to calculate the surface temperature of the monitored L-PBF process.

Sample images of both cameras and the quotient image of both camera images are shown in figure 4a-c. A layer of the printed cube sample with four sections of varying width with lower volume energy of E_V = -40 % can be seen.

In the sample images and mean gray values per layer of camera 1 and camera 2 (figure 4a,b,d,e) all sections with lower volume energy E_V are clearly recognizable by the lower gray values in these sections. In the sample quotient image (figure 4c), the sections with varied volume energy E_V are also visible, but the difference between varied sections and areas scanned with standard scanning parameters is less significant.

This can also be seen in the mean temperature values for the two marked sections for each layer of the build job in figure 4f. Shown as red dots are the mean temperature values for the red marked section with varied volume energy E_V, blue dots represent the mean temperature values for the blue marked section with standard parameters. The green lines represent the layers with varied volume energy E_V sections.

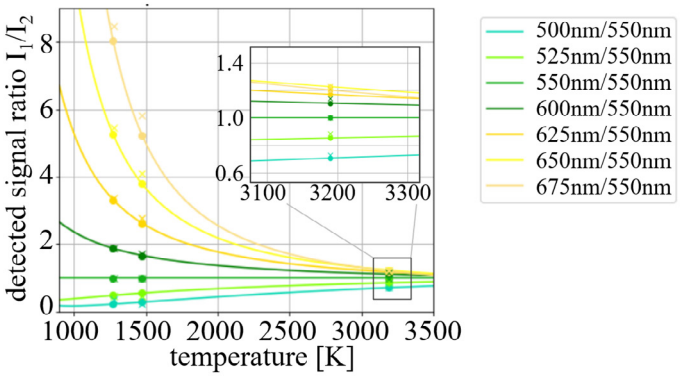

Fig. 3. Calculated intensity signal ratios I_1/I_2 for different bandpass filter combinations, compared with experimental measurements (crosses).

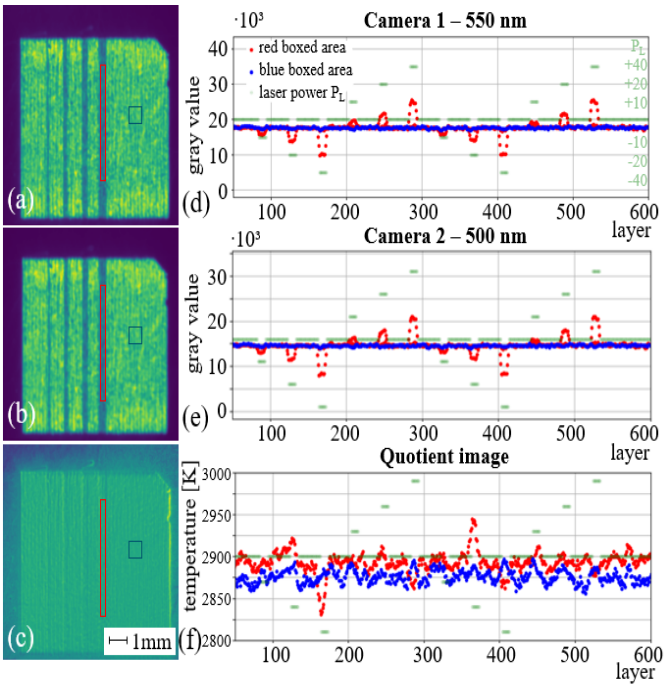

Fig. 4. (a) Sample images of the monitored L-PBF process, (b) mean gray values and resulting temperatures for two sections of the cube for all layers.

A mean maximum surface temperature of T = 2880 K can be seen for the printed cube. This is higher than the measured temperature by of Pavlov el. al. [8] and Furumotoa et. al. [9] but lower than the by means of simulation estimated surface temperatures of Khairallah et. al. [12]. They estimate maximum temperatures significantly above the boiling temperature of the used material.

No clear differentiation for different volume energy E_V can be made with the sensor set-up used in the initial experiment. The low significance of the quotient image can be traced back to the unfavorable choice of the bandpass filter combination.

Since the chosen bandpass filters 500 nm and 550 nm are close to each other, the measured signal intensity ratios I_1/I_2 range for monitored temperature differences become very small and is partly in the range of the signal noise. In fact, by applying a one-point temperature calibration as described by Altenburg et. al. [14] on the recorded images of one camera, the temperature deviation for a laser power variation of $L_P \pm 20$ % is $\Delta T \approx 100$ K. With the used filter combination, this corresponds to a signal difference of only 4 % and is thus not measurable with the current set-up due to calibration uncertainty, focus blurring and inaccurate image matching.

Consequently, other bandpass filter combination need to be chosen and tested for their applicability. From the presented data, e.g., a filter combination of 550 nm and 675 nm appears to be favorable.

To reach a better spatial resolution, the fine tuning of the individual camera focusing can be optimized, so that an additional median blurring of one image is no longer required. Also, the use of an industrial dual-wavelengths camera could minimize the measuring uncertainty due to the intrinsic accurate image matching. However, this step is only favorable after the determination of an optimum filter choice and when dual-wavelengths cameras with higher resolution are available.

5. Conclusion

In this paper, an approach for the surface temperature measurement with low-cost equipment in the visible light range by means of bi-chromatic optical tomography was presented.

The surface temperature of the L-PBF process for the nickel-based alloy used with a volume energy E_V = 51 MJ/mm³ could be estimated as T = 2880 K. Further comparative validation of this result needs to be done.

An initial experiment showed that further adaption of the sensor set-up is needed to measure temperature differences induced by volume energy changes. Other bandpass filter combinations will be tested since measurements of calibrated light sources showed promising results for several bandpass filter combinations.

Acknowledgements

Funded by: Federal Ministry for Economic Affairs and Climate Protection based on a resolution of the German Bundestag. The title of the project is “Active thermography with laser excitation for in-situ detection of defects during additive manufacturing in the metal powder bed process (16KN086124)”.

Special thanks to Frank Heinrichsdorff (Siemens AG) for the sample component design and Toni Räpke (BAM) for the scanning parameter.

References

[1] Wohlers associates, Inc. Wohlers Report 2021 - 3D Printing and Additive Manufacturing State of the Industry. ISBN 978-0-9913332-7-1. Washington, DC. 2022.

[2] Munsch, M.; Schmidt-Lehr, M.; Wycisk, E.; Führer, T. AMPOWER REPORT 2022 - Management Summary. Hamburg: AMPOWER GmbH & Co. KG. p. 5. 2022.

[3] Everton, S. K.; Hirsch, M.; et al. Review of in-situ process monitoring and in-situ metrology for metal additive manufacturing. Materials and Design. Volume 95. p. 431–445. 2016.

[4] McCann, R.; Obeidi, M. A.; Hughes, C.; et al. https://doi.org/10.1016/j.addma.2021.102058. Additive Manufacturing 45. 102058. 2021.

[5] Ladewig, A. Optische Tomographie - Online Prozessüberwachung für das selektive Laserschmelzen. Dissertation. Karlsruher Institut für Technologie, Karlsruhr. 2019.

[6] Mohr, G.; Altenburg, S.J.; et al. https://doi.org/10.3390/met10010103. Metals 10. 2020.

[7] Gögelein, A., Ladewig, A.; et al. Process Monitoring of Additive Manufacturing by Using Optical Tomography. 14th QIRT. 2018

[8] Pavlov, M.; Doubenskaia, M.; Smurov, I. https://doi.org/10.1016/j.phpro.2010.08.080. Physics Procedia. Volume 5. p. 523-531. 2010.

[9] Furumoto, T; Ueda, T.; et al. http://dx.doi.org/10.1016/j.cirp.2013.03.032. CIRP Annals. Volume 62. p. 223-226. 2013.

[10] Beckett, D. Boosting Additive Manufacturing Quality, Economics and Efficiency with Monitoring, Alerts and Diagnosis. Sigma labs Inc. ICAM2021. 2021.

[11] Hooper, A P. https://doi.org/10.1016/j.addma.2018.05.032. Additive Manufacturing 22. p. 548-559. 2018.

[12] Khairallah, S. A.; Anderson, A. T.; Rubenchik, A.; King, W. E. http://dx.doi.org/10.1016/j.actamat.2016.02.014. Acta Mater. Volume 108. p. 36–45. 2016.
[13] Mohr, G., Nowakowski, S., Altenburg, S. J., et. Al. https://doi.org/10.3390/met10111546. Metals 2020. Volume 10. Issue 11. 2020
[14] Altenburg, S. J., Straße, A., Gumenyuk, A., et. Al. https://doi.org/10.1080/17686733.2020.1829889. QIRT. Volume 19. P. 97-114. 202